HHS Public Access

Author manuscript

Muscle Nerve. Author manuscript; available in PMC 2018 November 01.

Published in final edited form as:

Muscle Nerve. 2017 November ; 56(5): 887–895. doi:10.1002/mus.25561.

Sensitivity distribution simulations of surface electrode configurations for electrical impedance myography

Seward Rutkove, M.D., **Adam Pacheck, B.S.**, and **Benjamin Sanchez, Ph.D.**

Department of Neurology, Beth Israel Deaconess Medical Center, Harvard Medical School, Boston, MA 02215-5491, USA.

Abstract

OBJECTIVE—Surface-based electrical impedance myography (EIM) is sensitive to muscle condition in neuromuscular disorders. However, the specific contribution of muscle to the obtained EIM values is unknown.

METHODS—We combined theory and the finite element method to calculate the electrical current distribution in a three-dimensional model using different electrode array designs and subcutaneous fat thicknesses (SFT). Through a sensitivity analysis, we decoupled the contribution of muscle from other surrounding tissues in the measured surface impedance values.

RESULTS—The contribution of muscle to surface EIM values varied greatly depending on the electrode array size and the SFT. For example, the contribution of muscle with 6 mm SFT was 8% for a small array versus 32% for a large array.

DISCUSSION—The approach presented can be employed to inform the design of robust EIM electrode configurations that maximize the contribution of muscle across the disease and injury spectrum.

Keywords

electrical impedance myography; electrophysiological measurement; electrodes; subcutaneous fat; muscle

Please address correspondence to: Benjamin Sanchez, Ph.D., Department of Neurology - Harvard Medical School Office DA-0730A, Beth Israel Deaconess Medical Center 330 Brookline Avenue, Boston, MA 02215-5491 USA, bsanchez@bidmc.harvard.edu, Phone: +1 617 667 3057.

Conflict of interest disclosure: Dr. Sanchez is named as an inventor on a patent application in the field of electrical impedance. Dr. Sanchez receives consulting income from Maxim Integrated, Inc. Dr. Rutkove has equity in, and serves a consultant and scientific advisor to, Skulpt, Inc. a company that designs impedance devices for clinical and research use; he is also a member of the company's Board of Directors. The company also has an option to license patented impedance technology of which Dr. Rutkove is named as an inventor. This study, however, did not employ any relevant company or patented technology.

Ethical publication statement: We confirm that we have read the Journal's position on issues involved in ethical publication and affirm that this report is consistent with those guidelines.

Author contributions

Conceived and designed the experiments: B.S. Performed the experiments: B.S., A.P. Analyzed the data: B.S., A.P. Wrote the paper: B.S., S.R. Revised and approved the manuscript: B.S., A.P., S.R.

Introduction

Electrical impedance myography (EIM) is an impedance-based technique for the assessment of neuromuscular disorders (NMD).[1] In its standard application, a set of four surface electrodes is placed on the skin over a muscle or muscle group of interest and the voltage resulting from the application of a high frequency and low-amplitude electric current is measured. Over the last two decades, a variety of studies have demonstrated EIM's ability to detect disease severity and track longitudinal changes in patients and animal models with NMD, including spinal muscular atrophy (SMA),[2] amyotrophic lateral sclerosis (ALS),[3] and Duchenne muscular dystrophy (DMD).[4]

Whereas the term “myography" in EIM's name implies that the technique assesses muscle condition alone, in fact, EIM's resistance and reactance values have contributions from all tissues underlying the electrodes. In the frequency range where EIM is typically measured (kHz to MHz), NMD alters the inherent dielectric properties of resistivity and relative permittivity of the muscle itself, which produces changes in the resistance and reactance values.[1] Moreover, EIM changes observed in progressive diseases likely reflect alterations in the size and shape of the muscle in relation to its surrounding tissues. For example, in a person with only modest subcutaneous fat and normal muscle bulk, much of the current applied flows through the muscle and relatively little through the skin, fat, and bone. However, in the same person with severe muscle atrophy, such as that which occurs in late-stage ALS, much of current would be expected to pass through non-muscular tissue. Therefore, the EIM technique using surface electrodes measures an apparent impedance (or equivalently an apparent resistance and an apparent reactance) that is, in general, related to but different from the muscle-specific impedance and the corresponding muscle-specific resistance and reactance.

However, measuring the muscle-specific impedance itself has additional value beyond that offered by the apparent impedance. For example, it becomes possible to detect alterations specifically due to disease-related changes in muscle histology that directly affect impedance measures including alterations in muscle fiber diameter, alignment, and surface membrane capacitance.[5] But in order to measure muscle-specific EIM values only, it would be necessary to place the four EIM electrodes in direct contact with the muscle. Moreover, that muscle would need to be perfectly homogeneous in its structure and of essentially infinite size, the latter so as to ensure the electric current could flow freely and without being affected by the volume of the muscle. Clearly these conditions are impossible to achieve in practice. Nevertheless, it is still possible to attempt to ensure that the measured apparent impedance is optimally enriched by the underlying muscle. To achieve this, electrode arrays can be designed -including designing the size and shape of individual electrodes and the inter-electrode distances- to maximize the contribution of muscle-specific alterations in the apparent impedance measured.

This situation is somewhat analogous to that of standard nerve conduction studies and measurement of surface recorded compound motor action potentials or sensory responses.[6,7] While we take these values to be representative of the electrical potentials generated by the underlying nerve or muscle, the absolute values that are recorded are the product of a variety

of additional factors including the thickness of subcutaneous fat and skin and volume conductor effects. Nevertheless, we are still able to adjust the active E1 and reference E2 electrodes as well as stimulation parameters to help maximize and standardize the resulting values with the goal of most effectively measuring the electrical properties of the underlying nerve and muscle.

The aim of this study is to advance surface EIM electrode designs by studying the specific contribution of muscle to the apparent surface impedance measured. To achieve this, we calculate the percentage contribution of muscle and other surrounding tissues to the EIM values using surface electrodes through the use of finite element models (FEMs). In order to do so, we first simulate subcutaneous fat and muscle tissues separately to establish their specific impedance values as measured using two electrode configurations employed by our research group in recent clinical studies. Next, we perform a "sensitivity" analysis to evaluate the "ability" of surface EIM technique to measure the specific impedance of underlying tissues. In doing so, we are able to decouple the impedance contribution of the skin, subcutaneous fat, muscle, and bone tissues with various electrode configurations and subcutaneous fat thicknesses.

Materials and methods

Finite element model simulations

Finite element model simulations were performed in the frequency domain using the AC/DC Module, Electric Currents Physics in Comsol Multiphysics software (Comsol, Inc, 5.2, Burlington, MA). For simplicity in the sensitivity analysis, we created a four-layer planar FEM rectangular slab with dimensions length l = 5 cm, width w = 10 cm, and height h = 4.5 cm consisting of skin h_s = 3 mm, subcutaneous fat h_{sf} from 2 to 20 mm (depending on the simulation), muscle h_m = 20 mm, and bone h_b from 2 to 20 mm. The number of points analyzed per dimension was N = 201 giving approximately 8.1 million regions within the conductor volume defined by the FEM model $V = l \cdot w \cdot h = 225\ cm^3$.

The dielectric properties in the x and z direction, i.e. relative permittivity $\varepsilon r^{[x,z]}$ and conductivity $\sigma^{[x,z]}$, were taken from a reference database created from the compilation of published data.[8–11] The properties of tissues considered are labeled in the database as "wet skin", "fat", "muscle", and "cortical bone" tissue properties. Directional dependence of "muscle" tissue properties in the longitudinal y direction (i.e. anisotropy) was determined from the transverse values as $\sigma\ m^{[y]} = 2\sigma\ m^{[x,z]}$ and $\varepsilon r,m^{[y]} = 0.1\varepsilon r,m^{[x,z]}$. Skin, subcutaneous fat and bone tissues were assumed to have isotropic properties.

The FEM was simulated at 51 frequencies distributed between 10 kHz and 1 MHz. Simulations with the small handheld electrode array shown in Fig.1 had a distance d = 1.2 cm between the midpoint of the inner electrodes. In order to evaluate the effect of different inter-electrode distances, the distance between centers of the inner and outer electrodes δ were varied across {0.6, 0.8, 1, 1.5, 2} times the distance between inner electrodes d (the inner voltage electrodes' distance remained unchanged). The large handheld electrode array in Fig.1 was only simulated with a uniform distance D = 2 cm between the midpoint of the electrodes. In all simulations, the electrode material was stainless steel with dimensions

width w_e = 5 mm and height h_e = 1 mm, relative permittivity ε_r = 1 (dimensionless) and real conductivity σ = 1.73913 MSm^{-1}. For the small and large arrays, electrode length was l_e = 15 mm and L_e = 25 mm., respectively.

The electrode nearest the coordinate reference point in the FEM was the current source electrode with I = 1 A the total current injected. Moving along the positive y-axis, the next two electrodes were the high and low voltage electrodes, respectively. The fourth electrode was the current sink electrode, modeled as a ground. The component of the electric current normal to all the outer boundaries was defined to be null to prevent the current flowing out of the boundaries defined by the model. Variations of the model changing subcutaneous fat thickness h_{sf} and electrode array separation were run using Comsol LiveLink toolbox via MATLAB (Mathworks, 2015a, Natick, MA).

Sensitivity analysis

We performed a "sensitivity" analysis to determine the contribution of each tissue from the model to the apparent impedance measured by surface electrodes. The sensitivity is determined by the combination of the following factors: electric current applied, conductor volumes and the tissues' dielectric properties, and electrode dimension, material, shape and disposition. The impedance sensitivity S in EIM can be calculated as follows[12]

$$S = J_1 \cdot J_2, \quad (1)$$

in m^{-4}, where J_1 and J_2 are the local current density vectors resulting from the application of an electric current between the outer two current surface electrodes and the inner two voltage surface electrodes, respectively. Depending on the relative orientation between the current density vectors, the sensitivity S can take values that are either positive, negative, or zero.

The apparent impedance measured Z in units of Ohms (Ω) then follows adding the resistivity ρ defined by the tissues' properties[13] weighted by the sensitivity, namely

$$Z = R + jX = \int_V (\rho \cdot J_1) \cdot J_2 \, dv, \quad (2)$$

where R and X are the resistance and reactance in Ω, and V is the total conductor volume in m^3. The impedance of each tissue in contributing to the measured impedance was then obtained by integrating the sensitivity values of the tissue over the volume it occupied. The apparent impedance Z values obtained using the sensitivity analysis were confirmed with those obtained using Ohm's law. Finally, the impedance of each tissue was normalized, dividing the resistance and reactance parts separately to obtain a quantitative measure of the tissue type contributing to the apparent impedance measured.

Physiological implications of sensitivity analysis: a numerical example

A sensitivity analysis gives the user an idea of the ability of EIM to measure muscle considering the effect of subcutaneous fat. To further illustrate this, we provide below a physiological interpretation of equation 2. Importantly, the values below are not representative of real data, but are chosen arbitrarily to exemplify the concept of impedance sensitivity. For simplicity, consider the apparent resistance (in lieu of the apparent reactance) of healthy muscle at 50 kHz is 100 Ω. Next, assume the sensitivity analysis reveals this resistance value is due to the contribution of four regions (see Fig.2A). According to equation 2, the resistance measured of healthy muscle is then

$$R_{\text{healthy}} = \underbrace{100\cdot(-0.3)}_{\text{skin, }-30\%} + \underbrace{200\cdot(0.3)}_{\text{sub.fat,}+60\%} + \underbrace{100\cdot(0.2)}_{\text{healthy muscle,}+20\%} + \underbrace{500\cdot(0.1)}_{\text{bone,}+50\%} = \underbrace{100}_{=100\%}\ \Omega.$$

Consider now the measurement of DMD muscle. The infiltration of less conductive adipose tissue increases the resistivity of diseased muscle (from 100 to 200 Ωm), which translates into an expected increase in the apparent resistance,

$$R_{\text{mild DMD}} = \underbrace{100\cdot(-0.3)}_{\text{skin, }-25\%} + \underbrace{200\cdot(0.3)}_{\text{sub.fat,}+50\%} + \underbrace{200\cdot(0.2)}_{\text{diseased muscle,}+33\%} + \underbrace{500\cdot(0.1)}_{\text{bone,}+42\%} = \underbrace{120}_{=100\%}\ \Omega.$$

Now, assume that the muscle is even more severely diseased (from 200 to 300 Ωm). But this time, the resistivity also increases in the region of negative sensitivity (from 100 to 200 Ωm). This would have the unexpected result of giving a lower apparent resistance value than in the mild case,

$$R_{\text{severe DMD}} = \underbrace{200\cdot(-0.3)}_{\text{skin, }-55\%} + \underbrace{200\cdot(0.3)}_{\text{sub.fat,}+55\%} + \underbrace{300\cdot(0.2)}_{\text{diseased muscle,}+55\%} + \underbrace{500\cdot(0.1)}_{\text{bone,}+45\%} = \underbrace{110}_{=100\%}\ \Omega.$$

This effect can potentially be so extreme as to cause the diseased-related change in the apparent resistance to go in the direction opposite that expected as shown here,

$$R_{\text{severe DMD}} = \underbrace{300\cdot(-0.3)}_{\text{skin, }-112\%} + \underbrace{200\cdot(0.3)}_{\text{sub.fat,}+75\%} + \underbrace{300\cdot(0.2)}_{\text{diseased muscle,}+75\%} + \underbrace{500\cdot(0.1)}_{\text{bone,}+63\%} = \underbrace{80}_{=100\%}\ \Omega.$$

The difference between this simple example and the reality is that, in practice, the apparent EIM values are due to the contribution of an infinite number of extremely small regions (see Fig.2B). These infinitely small regions are distributed within a three-dimensional conductor volume containing the volumes occupied from different tissues and fluids, each with different specific resistivity values. Each of these infinitely small regions will have associated a sensitivity value. If a region has zero sensitivity, this region will not contribute to the measured impedance. On the contrary, regions with large positive or negative sensitivity values will contribute more to the impedance measured. Regions of non-zero sensitivity may appear anywhere in the conductor volume, including the skin, subcutaneous fat and muscle tissues. Importantly, physiological changes occurring in regions of negative

sensitivity may limit the ability to distinguish healthy from diseased muscle by increasing/decreasing diseased-related changes (this also includes regions of negative sensitivity in the muscle, see Fig.2B). Further, these changes can confound the apparent values from healthy with diseased muscle and vice versa. We note that, as a result of the possibility of having negative sensitivity, the percentage contribution of tissues may exceed 100% of the value of the impedance, with the cumulative impedance always being 100% of the impedance measured.[14,15] Finally, the sum of total sensitivity within the volume occupied by a particular tissue will determine how much that tissue is contributing to the apparent EIM values.

Results

Muscle and subcutaneous fat impedance

First, we simulated subcutaneous fat and muscle tissue separately to establish their impedance values. The simulations were performed using the small handheld electrode array in Fig.1. The model dimensions were much greater than the electrode dimensions to avoid the impedance's being affected by the model volume or boundary conditions (Fig.3A). The resistance and reactance of subcutaneous fat are greater than those of muscle in longitudinal direction, with exception of the phase (Fig.3B). The characteristic frequency where the reactance of muscle is maximal is 331 kHz.

Apparent impedance

We then determined the apparent impedance values combining a four-layer planar FEM model including skin, subcutaneous fat, muscle and bone tissues with the same handheld electrode array as used in Fig.3. As expected, the apparent impedance measured including skin and subcutaneous fat tissues (Fig.4A) is different from the muscle-specific impedance in Fig.3. The characteristic frequency becomes 69 kHz for 6 mm, 48 kHz for 10 mm, and 40 kHz for 20 mm of subcutaneous fat thickness. We then simulated the effect of decreasing 20% the distance between the inner and outer electrodes from $\delta = d$ in Fig.4A to $\delta = 0.8d$ in Fig.4B. The distance between centers of the inner electrodes was $d = 1.2$ cm. Regardless of the subcutaneous fat thickness considered, bringing the current electrodes closer to the voltage electrodes[13] causes an increase in apparent resistance, reactance and phase values (Fig.4B). In this case, the apparent peak reactance frequency is 44 kHz for 6 mm, 33 kHz for 10 mm, and 30 kHz for 20 mm of subcutaneous fat thickness. We studied the effect of increasing the separation between the current and voltage electrodes below.

Sensitivity distribution

Data in Fig.5A and B plot the sensitivity distributions at 10 kHz in the region of interest defined by the xz-plane located at half the FEM volume's width, i.e. with coordinates $(x, y = w/2, z)$, for two arbitrary distances between the inner and outer electrodes: $\delta = 0.6d$ (Fig.5A) and $\delta = 2d$ (Fig.5B). Comparing visually both distributions, the reader can see the sensitivity in the muscle layer increases after increasing δ. In other words, the larger the distance between the inner and outer electrodes, the more the apparent impedance is determined by deeper tissue volumes. Note that in the cross-section evaluated in Fig.5, no negative

sensitivity values are observed (i.e. the sensitivity takes positive values from 0% –blue– to 100% –yellow–).

Also, the sensitivity field decreases in the skin and subcutaneous fat layers by increasing δ (highlighted by the color arrowheads). Fig.5C then compares the sensitivities of the previous electrode configurations δ = 0.6d in Fig.5A and δ = 2d in Fig.5B in one dimension only instead of a plane, i.e. along the depth in the center of both electrode arrays (x = l/2, y = w/2, z). By increasing the separation between the current and voltage electrodes, the penetration depth where the sensitivity drops below 10% increases from 7 mm to 13 mm and the sensitivity in the skin and subcutaneous fat layers decreases.

Individual tissue contribution to the apparent impedance

We then calculated the percentage contribution of skin, subcutaneous fat, muscle, and bone tissues, to the apparent impedance from the sensitivity distribution values. For the purpose of this study, expressing the contribution of tissues with a number offers an objective and quantitative way to compare outcomes through EIM simulation studies. The values reported in Tables 1 and 2 correspond to the apparent impedance values in Fig.4A and B at 10 kHz and 52.48 kHz, respectively.

Simulating the small handheld electrode array in Fig.4A (4.6 cm in length), the muscle contributes 12% to the apparent resistance at 10 kHz with 6 mm of subcutaneous fat thickness (Table 1). The contribution of muscle decreases to 8% at 52.48 kHz. As regards the reactance, the muscle contribution at 10 kHz and 52.48 kHz is 118% and 15%, respectively. With electrode array configuration simulated in Fig.4B, the contribution of muscle to the apparent resistance and reactance is 8% and 11% at 10 kHz (Table 2). At 52.48 kHz, these percentages decrease to 6% and 8%, respectively. With the large electrode array (7 cm in length), the contribution of muscle to the resistance increases to 32% at 52.48 kHz (see Supplementary Table 1).

Note that because the total sensitivity may be negative in the volume occupied by tissue, the percentage contribution of tissues with positive sensitivity may be higher than 100%. In the end, however, the apparent impedance calculated with sensitivity has to be equal (100%) to the apparent impedance measured using Ohm’s law.

Discussion

The contribution of muscle and other tissues to the apparent impedance measured, hereafter termed simply as impedance, is difficult to determine experimentally. One approach is to solve the problem analytically using theoretical models.[17–19] Another approach is to measure impedance phantoms.[20] The difficulty of these two methods, however, lies in measuring realistic geometries with anisotropic tissues using electrodes that are not simply point sources. A more tractable approach to study their relationship is to use a FEM model that describes the reality as accurately as possible while still maintaining a limited number of simulation parameters.

Due to the complex reasons mentioned above, previous experimental studies have relied on statistics to evaluate the effect of subcutaneous fat from the impedance measured with surface electrodes.[21,22] These studies simplified the problem using empirical linear correlations between impedance values and the thickness of subcutaneous fat; the latter obtained using ultrasound techniques. Here, we studied the changes in impedance through FEM simulations after intentionally varying only the subcutaneous fat thickness and surface electrode configuration. This is a major difference with respect to experimental studies, where changes in impedance could be originated by experimental errors[23-28] and other physiological factors beyond solely subcutaneous fat thickness. Importantly, the lack of standard measurement protocols across all previous experimental studies and knowledge of the in vivo tissue dielectric properties makes it impossible to perform a direct comparison to the values reported here. In addition, compared to previous EIM studies that used FEMs, the authors did not assess the actual percentage contribution of muscle to the impedance values with these different electrode designs.[16,29]

An important result from this study is that the sensitivity distribution of surface electrode configurations for EIM may obtain regions of negative sensitivity.[14,15] The concept of negative impedance sensitivity can help the reader to interpret changes in diseased EIM values. For example, in Li et al,[30] the authors found the apparent resistance values were higher in older compared with younger muscular dystrophy (mdx) mice. This result was opposite to that expected because older mdx mice had an increased infiltration in muscle of connective tissue, which has a resistivity lower than that of muscle. One possible explanation is that the infiltration of connective tissue in old mdx muscle happened in a region with negative impedance sensitivity, thus producing a result opposite of that expected.

Here, we have shown one approach to increase the percentage contribution of muscle is to increase the separation between the current electrodes while keeping fixed the distance between the inner voltage electrodes. An alternative approach would be to keep the current electrode distance constant and move the voltage electrodes together. In the end, a compromise must be found in electrode array design to balance the depth of penetration to increase the contribution of muscle and to ensure a minimal measurable length of muscle. This issues become especially relevant when measuring small muscles, such as the intrinsic hand muscles of adults or virtually any appendicular muscle in an infant.[31,32]

The sensitivity distribution simulations presented can help to improve electrode physical characteristics to intentionally increase the contribution of muscle. Still, care should be taken interpreting the contribution of each tissue to the impedance values reported here; there are important assumptions that may limit the clinical impact of our findings. First, our model did not consider the shape of the muscle. Second, other fluids such as subcutaneous fat tissue blood flow were not included in the model. Third, the ex vivo dielectric data simulated may not be representative of in vivo dielectric data. Finally, we did not simulate practical limitations of the EIM technique such as the effects of electrode-skin interface on the impedance.

The results presented are especially relevant in explaining some of the cross-sectional variation amongst healthy subjects when measuring surface EIM. It is likely that variations

in subcutaneous fat thickness, muscle size and shape all alter sensitivity distributions, contributing to differences in the relative contribution of muscle measured. However, previous human and animal studies have shown that non-optimized impedance measures can still serve as reliable surrogate measures for evaluating NMD status, with a moderate to strong correlation between surface EIM values and standard neurophysiological, functional, and histological measures in a variety of conditions.[33,34]

This study highlights the importance of finite element modeling and sensitivity theory as two separate but related approaches for improving the design of electrodes arrays. Combining both modalities in the development of future electrode designs will ensure that EIM sensitivity to muscle status is optimized.

Supplementary Material

Refer to Web version on PubMed Central for supplementary material.

Acknowledgements

The authors are thankful to Dr. Hyeuknam Kwon from Yonsei University, Seoul, Korea for his comments on the paper.

Financial disclosure: This work was supported by NIH grant K24 NS060951.

Abbreviations list

EIM	Electrical impedance myography
SFT	Subcutaneous fat thickness
NMD	Neuromuscular disorders
FEM	Finite element model

References

[1]. Sanchez B, Rutkove SB. Electrical Impedance Myography and Its Applications in Neuromuscular Disorders. Neurotherapeutics. Nov.2016 :1–12. [PubMed: 26684870]

[2]. Rutkove SB, Shefner JM, Gregas M, Butler H, Caracciolo J, Lin C, et al. Characterizing spinal muscular atrophy with electrical impedance myography. Muscle Nerve. Dec; 2010 42(6):915–21. [PubMed: 21104866]

[3]. Rutkove SB, Caress JB, Cartwright MS, Burns TM, Warder J, David WS, et al. Electrical impedance myography as a biomarker to assess ALS progression. Amyotroph. lateral Scler. Sep; 2012 13(5):439–45. [PubMed: 22670883]

[4]. Rutkove SB, Geisbush TR, Mijailovic A, Shklyar I, Pasternak A, Visyak N, et al. Cross-sectional evaluation of electrical impedance myography and quantitative ultrasound for the assessment of Duchenne muscular dystrophy in a clinical trial setting. Pediatr. Neurol. Jul; 2014 51(1):88–92. [PubMed: 24814059]

[5]. Eisenberg, RS. In Compr. Physiol. John Wiley & Sons, Inc; 1980. Impedance Measurement of the Electrical Structure of Skeletal Muscle; p. 301-323.

[6]. Van Dijk JG, Van der Kamp W, Van Hilten BJ, Van Someren P. Inuence of recording site on CMAP amplitude and on its variation over a length of nerve. Muscle Nerve. 1994; 17(11):1286–1292. [PubMed: 7935551]

[7]. Bromberg MB, Spiegelberg T. The influence of active electrode placement on CMAP amplitude. Electroencephalogr. Clin. Neurophysiol. Oct; 1997 105(5):385–9. [PubMed: 9363004]

[8]. Gabriel C, Gabriel S, Corthout E. The dielectric properties of biological tissues: I. Literature survey. Phys. Med. Biol. Nov; 1996 41(11):2231–49. [PubMed: 8938024]

[9]. Gabriel S, Lau RW, Gabriel C. The dielectric properties of biological tissues: II. Measurements in the frequency range 10 Hz to 20 GHz. Phys. Med. Biol. Nov; 1996 41(11):2251–2269. [PubMed: 8938025]

[10]. Gabriel S, Lau RW, Gabriel C. The dielectric properties of biological tissues: III. Parametric models for the dielectric spectrum of tissues. Phys. Med. Biol. Nov; 1996 41(11):2271–93. [PubMed: 8938026]

[11]. Andreuccetti, D., Fossi, R., Petrucci, C. An Internet resource for the calculation of the dielectric properties of body tissues in the frequency range 10 Hz - 100 GHz. 1997.

[12]. Geselowitz DB. An application of electrocardiographic lead theory to impedance plethysmography. IEEE Trans. Biomed. Eng. 1971; 18(1):38–41. [PubMed: 5545046]

[13]. Malmivuo, J., Plonsey, R. Bioelectromagnetism: Principles and Applications of Bioelectric and Biomagnetic Fields. Vol. ume 20. Oxford University Press; 1995.

[14]. Plonsey R, Collin R. Electrode guarding in electrical impedance measurements of physiological systems: a critique. Med. Biol. Eng. Comput. Sep; 1977 15(5):519–527. [PubMed: 199806]

[15]. Penney BC. Theory and cardiac applications of electrical impedance measurements. Crit. Rev. Biomed. Eng. 1986; 13(3):227–81. [PubMed: 3516573]

[16]. Jafarpoor M, Li J, White JK, Rutkove SB. Optimizing electrode configuration for electrical impedance measurements of muscle via the finite element method. IEEE Trans. Biomed. Eng. May; 2013 60(5):1446–52. [PubMed: 23314763]

[17]. Robillard PN, Poussart D. Spatial resolution of four electrode array. IEEE Trans. Biomed. Eng. Aug; 1979 26(8):465–70. [PubMed: 468292]

[18]. Suesserman M, Spelman F. Quantitative in vivo measurements of inner ear tissue resistivities. I. In vitro characterization. IEEE Trans. Biomed. Eng. 1993; 40(10):1032–1047. [PubMed: 8294128]

[19]. Steendijk P, Mur G, Van Der Velde ET, Baan J. The four-electrode resistivity technique in anisotropic media: theoretical analysis and application on myocardial tissue in vivo. IEEE Trans. Biomed. Eng. Nov; 1993 40(11):1138–48. [PubMed: 8307598]

[20]. Naydenova E, Cavendish S, Wilson A. Measurement and modelling the sensitivity of tetrapolar transfer impedance measurements. Med. Eng. Phys. Jul.2016 :1–10. 0(0).

[21]. Schwartz S, Geisbush TR, Mijailovic A, Pasternak A, Darras BT, Rutkove SB. Optimizing electrical impedance myography measurements by using a multifrequency ratio: A study in Duchenne muscular dystrophy. Clin. Neurophysiol. 2015; 126(1):202–208. [PubMed: 24929900]

[22]. Li L, Li X, Hu H, Shin H, Zhou P. The Effect of Subcutaneous Fat on Electrical Impedance Myography: Electrode Configuration and Multi-Frequency Analyses. PLoS One. Jan.2016 11(5):e0156154. [PubMed: 27227876]

[23]. Al-Hatib F. Patient-instrument connection errors in bioelectrical impedance measurement. Physiol. Meas. May; 1998 19(2):285–96. [PubMed: 9626692]

[24]. Bolton MP, Ward LC, Khan A, Campbell I, Nightingale P, Dewit O, et al. Sources of error in bioimpedance spectroscopy. Physiol. Meas. 1998; 235(19):235–245.

[25]. Scharfetter H, Hartinger P, Hinghofer-Szalkay H, Hutten H. A model of artefacts produced by stray capacitance during whole body or segmental bioimpedance spectroscopy. Physiol. Meas. May; 1998 19(2):247–61. [PubMed: 9626689]

[26]. Buendia R, Seoane F, Gil-Pita R. Experimental validation of a method for removing the capacitive leakage artifact from electrical bioimpedance spectroscopy measurements. Meas. Sci. Technol. Nov.2010 21(11):115802.

[27]. Bogonez-Franco P, Nescolarde L, Bragos R, Rosell-Ferrer J, Yandiola I. Measurement errors in multifrequency bioelectrical impedance analyzers with and without impedance electrode mismatch. Physiol. Meas. Jul; 2009 30(7):573–87. [PubMed: 19491458]

[28]. Sanchez B, Pacheck A, Rutkove S. Guidelines to electrode positioning for human and animal electrical impedance myography research. Sci. Rep. 2016; 6(32615):1–14. [PubMed: 28442746]

[29]. Wang L, Ahad M, McEwan A, Li J, Jafarpoor M, Rutkove S. Assessment of alterations in the electrical impedance of muscle after experimental nerve injury via finite element analysis. IEEE Trans. Biomed. Eng. Jan; 2011 58(6):1585–1591. [PubMed: 21224171]

[30]. Li J, Geisbush TR, Rosen GD, Lachey J, Mulivor A, Rutkove SB. Electrical impedance myography for the in vivo and ex vivo assessment of muscular dystrophy (mdx) mouse muscle. Muscle Nerve. Jun; 2014 49(6):829–35. [PubMed: 24752469]

[31]. Zaidman CM, Wang LL, Connolly AM, Florence J, Wong BL, Parsons JA, et al. Electrical impedance myography in Duchenne muscular dystrophy and healthy controls: A multicenter study of reliability and validity. Muscle Nerve. Oct; 2015 52(4):592–7. [PubMed: 25702806]

[32]. Kolb SJ, Coffey CS, Yankey JW, Krosschell K, Arnold WD, Rutkove SB, et al. Baseline results of the NeuroNEXT spinal muscular atrophy infant biomarker study. Ann. Clin. Transl. Neurol. 2016; 3(2):132–45. [PubMed: 26900585]

[33]. Wang LL, Spieker AJ, Li J, Rutkove SB. Electrical impedance myography for monitoring motor neuron loss in the SOD1 G93A amyotrophic lateral sclerosis rat. Clin. Neurophysiol. Dec; 2011 122(12):2505–11. [PubMed: 21612980]

[34]. Rutkove SB, Caress JB, Cartwright MS, Burns TM, Warder J, David WS, et al. Electrical impedance myography correlates with standard measures of ALS severity. Muscle and Nerve. 2014; 49(3):441–443. [PubMed: 24273034]

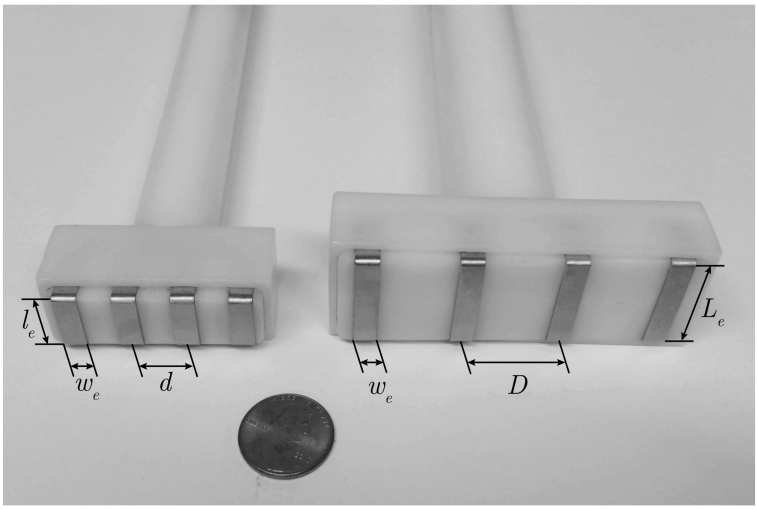

Figure 1.

Examples of handheld electrode arrays used for electrical impedance myography measurements in humans and simulated in this study. The small and large electrodes' arrays are made of stainless steel metal strips with identical width w_e = 5 mm and height h_e = 1 mm (dimension not shown). The uniform center distances between electrodes are d = 1.2 cm and D = 2 cm, while the lengths of electrodes are l_e = 15 mm and L_e = 25 mm.

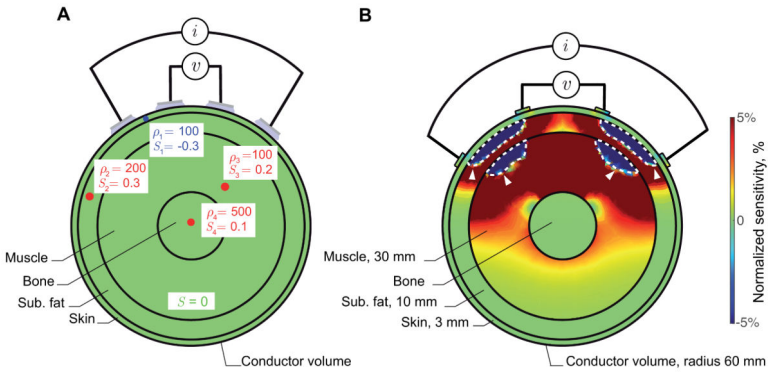

Figure 2.

(A) Numerical example of an electrical impedance myography (EIM) measurement where the current (i) and voltage (v) surface EIM electrodes are in contact with a conductor volume with positive (red), zero (green), and negative (blue) sensitivity S regions in the skin, subcutaneous fat, muscle and bone. The contribution of the four regions determines the surface resistance measured. (B) Cross section view of the sensitivity distribution simulation of a cylinder-shaped finite element model. The white arrowheads indicate regions of negative sensitivity in subcutaneous fat and muscle tissues.

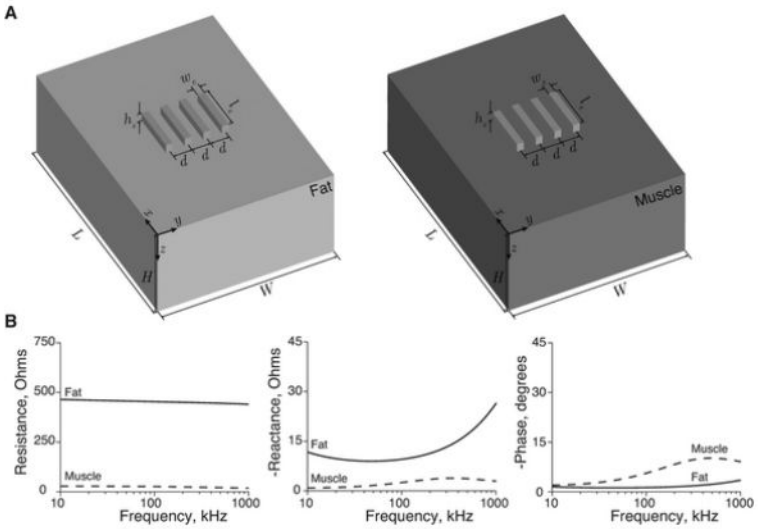

Figure 3.

Subcutaneous fat and muscle impedance values simulating the small handheld electrode array in Fig.1. (A) Subcutaneous fat and muscle's finite element models are considered. The volume dimensions are L = 50 cm, W = 100 cm, and H = 20 cm. The electrodes are placed in contact with each tissue separately, with relative permittivity $\varepsilon_r = 1$ and conductivity $\sigma = 1.73913\ \mathrm{MSm}^{-1}$. (B) Reference subcutaneous fat and longitudinal muscle impedance values.

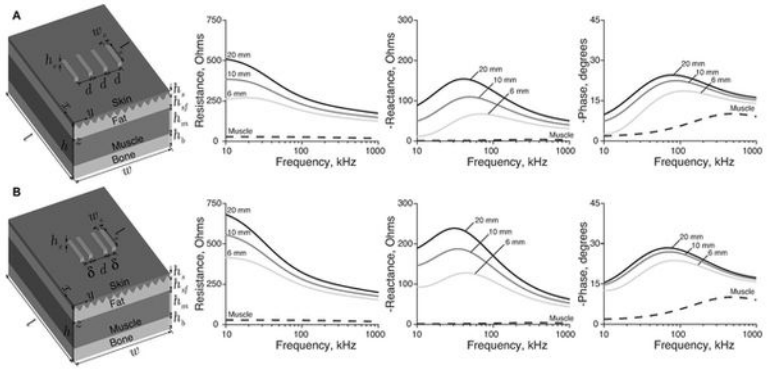

Figure 4.

Apparent impedance including skin, subcutaneous fat, muscle and bone tissues. The volume dimensions of the four-layer finite element models are l = 5 cm, w = 10 cm, h = 4.5 cm including the thickness of skin h_s = 3 mm, subcutaneous fat h_{sf} from 6 to 20 mm, muscle h_m = 20 mm, and bone h_b from 2 to 18 mm. The complex resistivity of skin, ρ_s; subcutaneous fat, ρ_{sf} ; muscle, ρ_m; and bone, ρ_b; are simulated from 10 kHz to 1 MHz. (A) Impedance spectra with varying subcutaneous fat thicknesses h_{sf} simulating the small handheld electrode array in Fig.3 with evenly spaced electrodes d; and (B) with $\delta = 0.8d$ the distance between the inner and outer electrodes. The specific muscle impedance from Fig.3 is shown in dotted lines for comparison purposes with the apparent impedance.

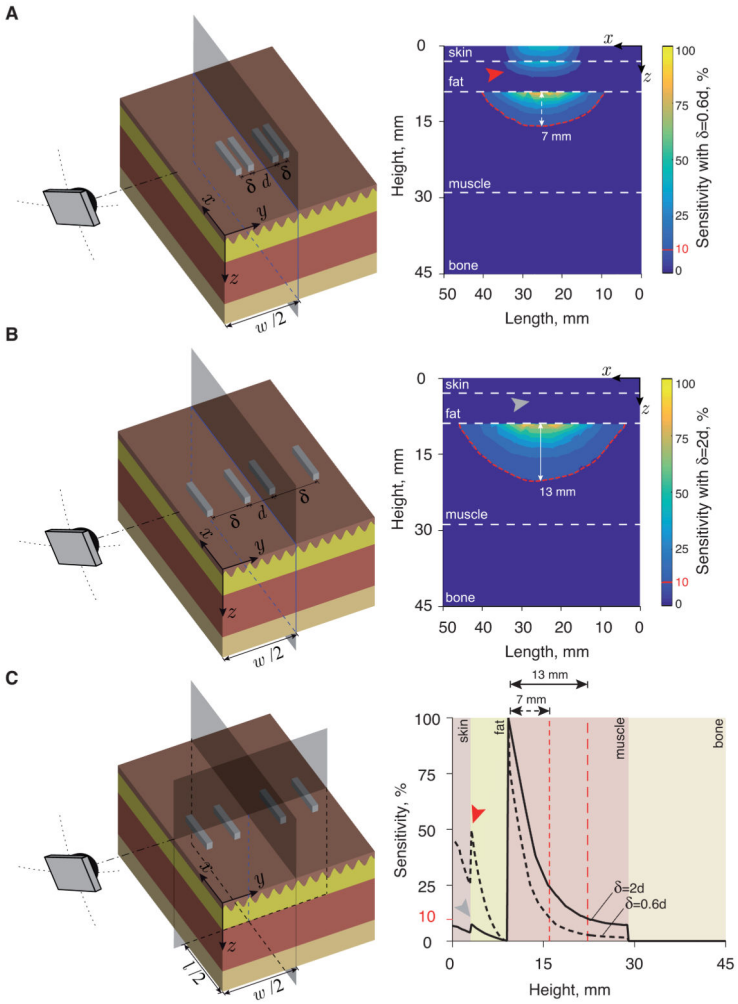

Figure 5.

Sensitivity distribution of surface electrical impedance measurements with h_{sf} = 6 mm subcutaneous fat thickness at 10 kHz. The surface electrode array is placed over the skin (height z= 0 mm) centered in the y direction. Examples of sensitivity fields in xz-plane (delimited by the blue dotted lines) located at half the volume width (x, w/2, z) for two current-voltage surface electrode configurations: δ = 0.6d (A) and δ = 2d (B). The sensitivity field was normalized to its maximum value in the xz-plane. The camera illustrates the position of the viewer for the three-dimensional plot. (C) Sensitivity field comparison of electrodes configurations δ = 0.6d (A) and δ = 2d (B) along the z-axis only (denoted by the blue dotted line) with coordinates (l/2, w/2, z). The depth of penetration with 10% sensitivity increased from 7 mm with δ = 0.6d (A) to 13 mm with δ = 2d (B).

Table 1

Sensitivity analysis of the apparent resistance R and reactance X measured using the small handheld electrode array with uniformly spaced electrodes in Fig.4A.

		10 kHz			52.48 kHz		
		Subcutaneous fat thickness			Subcutaneous fat thickness		
		6 mm	10 mm	20 mm	6 mm	10 mm	20 mm
$R\,(\Omega)$	Skin	−29 (−11%)	−4 (−1%)	31 (6%)	72 (31%)	120 (42%)	166 (48%)
	Sub. fat	256 (98%)	369 (96%)	468 (92%)	141 (61%)	151 (53%)	173 (50%)
	Muscle	31 (12%)	23 (6%)	10 (2%)	19 (8%)	11 (4%)	7 (2%)
	Bone	0 (0%)	0 (0%)	0 (0%)	0 (0%)	0 (0%)	0 (0%)
	Apparent	258	388	509	231	282	346
$-X\,(\Omega)$	Skin	−14 (−116%)	−46 (−91%)	−68 (−77%)	−55 (−85%)	−43 (−39%)	−30 (−20%)
	Sub. fat	12 (98%)	90 (180%)	154 (175%)	111 (170%)	146 (134%)	178 (118%)
	Muscle	14 (118%)	6 (11%)	2 (2%)	10 (15%)	7 (6%)	3 (2%)
	Bone	0 (0%)	0 (0%)	0 (0%)	0 (0%)	0 (0%)	0 (0%)
	Apparent	12	50	88	66	110	151

Table 2

Sensitivity analysis of the apparent resistance R and reactance X measured using the electrode array with non-uniformly spaced electrodes in Fig.4B.

		10 kHz			52.48 kHz		
		Subcutaneous fat thickness			Subcutaneous fat thickness		
		6 mm	10 mm	20 mm	6 mm	10 mm	20 mm
$R\,(\Omega)$	Skin	0 (0%)	39 (7%)	82 (12%)	133 (44%)	189 (53%)	235 (57%)
	Sub. fat	382 (92%)	495 (89%)	593 (87%)	152 (50%)	157 (44%)	169 (41%)
	Muscle	33 (8%)	22 (4%)	7 (1%)	18 (6%)	11 (3%)	4 (1%)
	Bone	0 (0%)	0 (0%)	0 (0%)	0 (0%)	0 (0%)	0 (0%)
	Apparent	415	556	682	303	357	408
$-X\,(\Omega)$	Skin	−14 (−15%)	−52 (−36%)	−81 (−43%)	−39 (−31%)	−18 (−10%)	−4 (−2%)
	Sub. fat	97 (104%)	193 (133%)	269 (143%)	155 (123%)	189 (107%)	221 (101%)
	Muscle	10 (11%)	6 (4%)	2 (1%)	10 (8%)	5 (3%)	2 (1%)
	Bone	0 (0%)	0 (0%)	0 (0%)	0 (0%)	0 (0%)	0 (0%)
	Apparent	93	147	190	126	177	219